Analytical Biochemistry 646 (2022) 114628

Contents lists available at ScienceDirect

Analytical Biochemistry

journal homepage: www.elsevier.com/locate/yabio

A stable enzyme sensor via embedding enzymes into zeolitic imidazolate frameworks for pesticide determination

Yisong Zhao, Xiong Lu, Faming Gao *

Key Laboratory of Applied Chemistry, College of Environmental and Chemical Engineering, Yanshan University, Qinhuangdao, 066004, China

ARTICLE INFO

Keywords:
Biomimetic mineralization
Stable electrochemical biosensor
Pesticide determination

ABSTRACT

The stability of biosensors is of significant importance for practical applications, and the natural biomineralization processes in living organisms have inspired us from a new perspective. In this work, acetylcholinesterase (AChE) was embedded into zeolitic imidazolate framework-8 carriers (with negligible cytotoxicity) via biomimetic mineralization, being demonstrated to be a stable strategy for enzyme immobilization. When further coupled with the conductive and catalytic Au nanoparticles, the biocomposites were explored as electrochemical pesticide detection biosensor, which showed favorable analytical performance, and improved stability comparing with other biosensors. This work provides a new strategy for the reasonable design of stable biosensors for different analytes monitoring.

1. Introduction

Organophosphorus pesticides (OPs) are commonly utilized in agriculture as insecticides and herbicides with high efficiency [1,2]. However, the toxic pesticides would not only contaminate the environment and foods [3], but also seriously threaten human health by irreversibly inhibit the activity of acetylcholinesterase (AChE) in the central nervous system [4]. Hence, it is essential to establish applicable pesticides detection systems.

Electrochemical biosensors based on AChE have been developed as a promising alternative method for pesticides analysis owing to their simple operation, low cost, high efficiency and on-site testing [5–7]. For this kind of biosensor, AChE could catalyze the breakdown of acetylthiocholine chloride (ATCh) into the electroactive material of thiocholine (TCh), which can be monitored via the irreversible oxidation current. And inhibition of the enzymatic activity by organophosphorus pesticides will cause the reduction in the current response of TCh, which can be served as a label for OPs determination. And the immobilization of enzyme is of significant importance in fabricating AChE biosensors. Traditional enzyme immobilization techniques include cross-linking, adsorption, entrapment, etc [8]. Combining these enzyme immobilization methods with advanced nanomaterials, novel AChE biosensors have been successfully explored [9–12]. However, in the construction of practical AChE biosensors, it is pivotal to effectively immobilize AChE meanwhile maintaining the activity of enzyme. And the stability is another key aspect to evaluate the applicability of the biosensors, which still needs to be improved for practical detections. Recently, metal-organic frameworks (MOFs), especially zeolitic imidazolate frameworks (ZIFs), have been used to immobilize biomolecules because of the mild synthesis conditions, robust systems, the high surface area and pore volume [13–17]. The organic linkers with special functional groups (e.g. the imidazole group in ZIFs) or metal ions tend to nucleate around biomolecules, accelerate the biomineralization process and produce stable biocomposites [16,18]. Due to the confinement effect, specific host-guest interactions and negligible cytotoxicity [18–21], ZIFs not only preserve the bioactivity of biomolecules [19,21,22], but also enhance their stability during usage [23–26]. Therefore, when ZIFs are exploited to construct enzyme biosensors, they are anticipated to improve the durability of biosensors.

Herein, the effectiveness of using porous ZIF-8 framework as AChE encapsulation and immobilization matrix to develop an AChE biosensor for malathion monitoring was investigated (Scheme 1). The AChE@ZIF-8 biocomposites, synthesized via biomineralization, possessed large surface area, high porosity and good biocompatibility, which offered proper microenvironment for enzymes. When further combined with the electro-conductive and catalytic gold nanoparticles, the as-fabricated biosensor exhibited satisfying sensitivity and a low detection limit for malathion, as well as enhanced stability and good reproducibility. This research provided a new enzyme immobilization way to build stable biosensors for pesticides detection.

* Corresponding author.
E-mail address: fmgao@ysu.edu.cn (F. Gao).

https://doi.org/10.1016/j.ab.2022.114628
Received 9 December 2021; Received in revised form 14 February 2022; Accepted 22 February 2022
Available online 4 March 2022

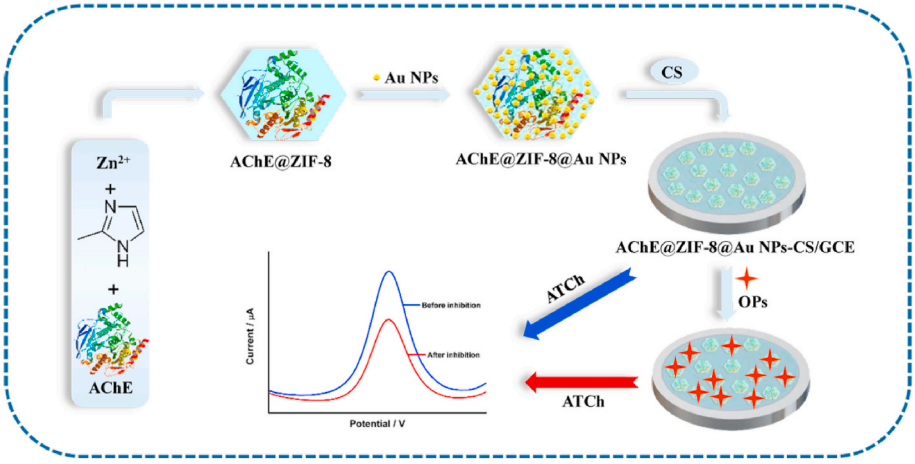

Scheme 1. Procedure for fabricating AChE@ZIF-8@Au NPs biosensor for pesticides detection.

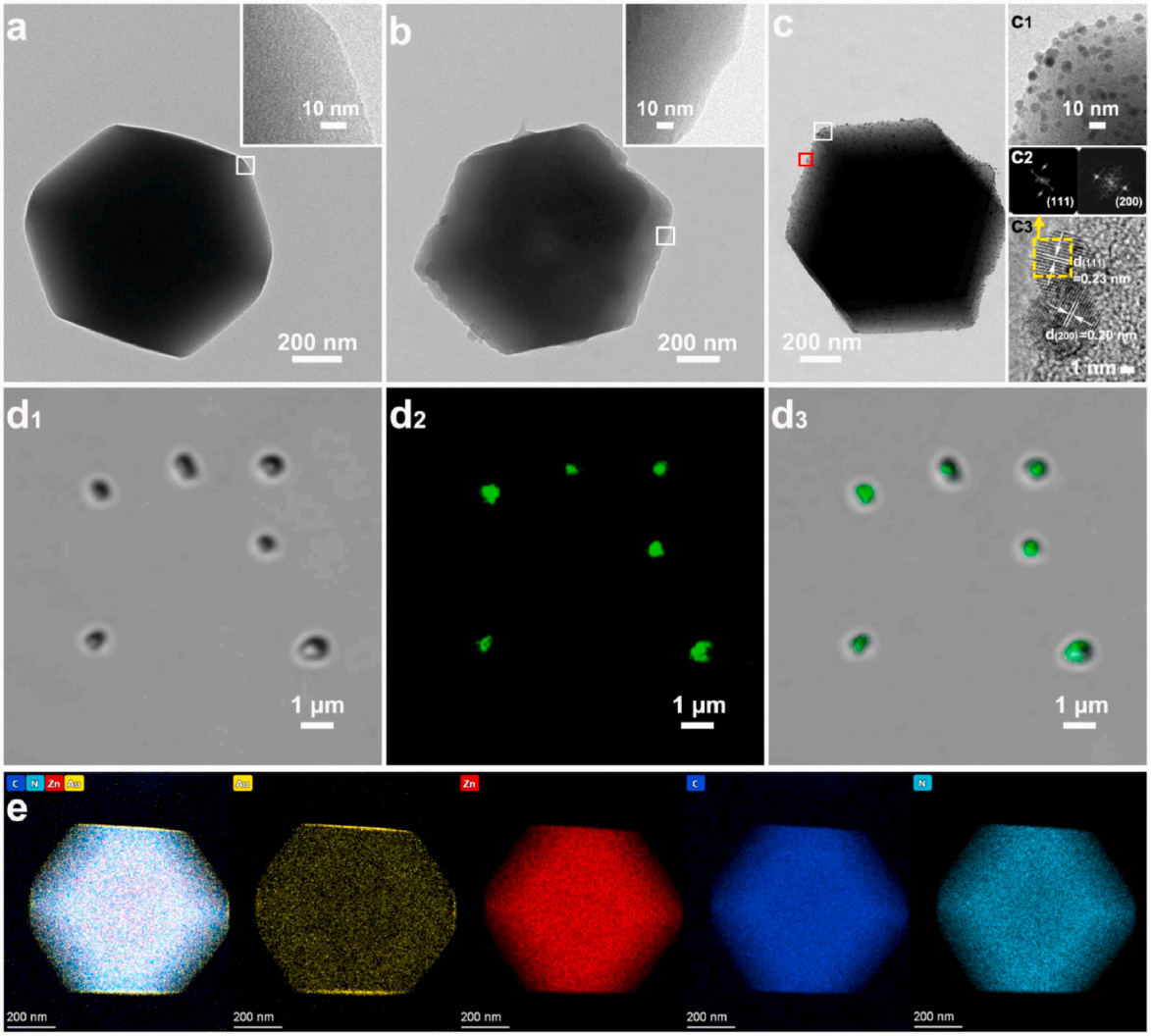

Fig. 1. TEM images of (a) ZIF-8, (b) AChE@ZIF-8, (c) AChE@ZIF-8@Au NPs. Confocal microscopy images of FITC-labelled AChE@ZIF-8 (d): bright-field microscopy image of the ZIF-8 (d_1); green fluorescence of the FITC-labelled AChE (d_2); and the merged image (d_3). Inset a and b are partial magnified detailed TEM images of the white box area in (a) and (b); (c_1) is a partial magnified detailed TEM image of the white box area in (c), (c_3) is the HRTEM image of the red box area in (c) and (c_2) is the corresponding fast fourier transform view of (c_3). Elemental mapping images (e). (For interpretation of the references to colour in this figure legend, the reader is referred to the Web version of this article.)

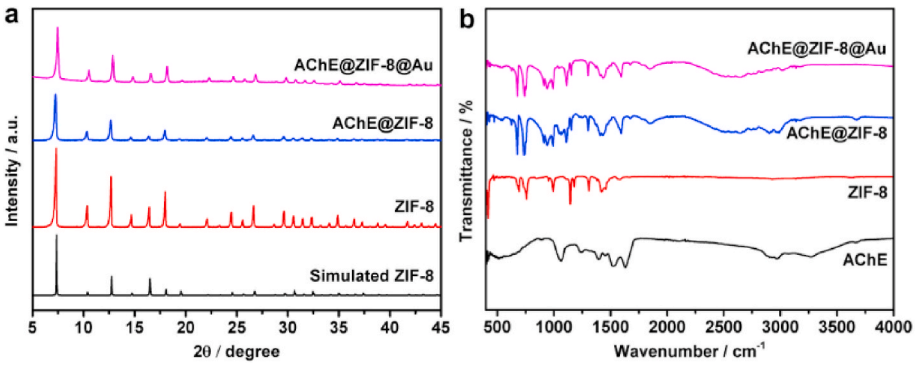

Fig. 2. XRD and FTIR spectra of different materials.

2. Experimental

2.1. Reagents and characterization methods

Acetylthiocholine chloride (ATCh, ≥ 99%), AChE (500 U/mg), fluorescein isothiocyanate isomer I (FITC, ≥ 90%), chloroauric acid and chitosan (85% deacetylation) were purchased from Sigma Aldrich. Zinc acetate, 2-methylimidazole and sodium borohydride were provided by Aladdin. Malathion was bought from LGC Promochem (Wesel, Germany). Ultrapure water was employed during the whole experiment.

The morphology of the nanomaterials was characterized by transmission electron microscopy (TEM, Hitachi HT7700) with energy dispersive spectrometer (EDS) and high-resolution TEM (HRTEM, FEI Tecnai F30). Confocal microscopy images of the FITC-labelled AChE encapsulated in MOFs were investigated by confocal laser scanning microscopy (CLSM, ZEISS LSM 710). The structure of synthesized materials was analyzed by powder x-ray diffraction (XRD, D/MAX-2500). Three-electrode system, that is the platinum foil (auxiliary electrode), the saturated calomel electrode (reference electrode) and the bare or modified glass carbon electrode (working electrode), was employed for electrochemical tests, which were performed using the electrochemical workstation (CHI750E). N_2 adsorption–desorption isotherms were measured at 77 K on a Micromeritics ASAP 2460 analyzer. Fourier transform infrared spectroscopy (FTIR) was analyzed using FT-IR NICOLET iS10.

2.2. Preparation of AChE@ZIF-8 and AChE@ZIF-8@Au NPs biocomposites

AChE@ZIF-8 biocomposites were synthesized via biomineralization using a modified aqueous solution synthesis method: Firstly, 20 μL AChE (1.25 U/μL) was mixed with 0.1 mL zinc acetate (0.31 M) solution and stirred gently for 20 min (25 °C). Secondly, 1 mL 2-methylimidazole (1.25 M) solution was quickly added to the above solution, the obtained solution was then stirred continuously for 2 h at room temperature. Finally, the synthesized AChE@ZIF-8 biocomposites were washed with ultrapure water, and 3 cycles of centrifugation (4000 rpm, 10 min) were executed. The obtained materials were redissolved in water or freeze-dried for further use. FITC-labelled AChE@ZIF-8 biocomposites were subjected to the identical procedure to synthesize the AChE@ZIF-8, and ZIF-8 was prepared the same way but without enzyme.

AChE@ZIF-8@Au NPs biocomposites were prepared as follows: 50 μL 10 mM $HAuCl_4$ solution (0.5 mmol) was dispersed in 500 μL AChE@ZIF-8 solution, then 50 μL 10 mM $NaBH_4$ solution was injected dropwise within 1 h, after that the reaction mixture was kept vibrating overnight (25 °C), eventually the AChE@ZIF-8@Au NPs biocomposites were obtained. ZIF-8@Au NPs nanocomposites were prepared similarly.

2.3. Fabrication of different biosensors

Chitosan (CS) as a biocompatible, adhesive, and positively charged polymer, is utilized for the fabrication of different biosensors, further improving the matrix mechanical stability and the immobilization efficiency for the negatively charged AChE [1].

First of all, the glass carbon electrode (GCE, with a diameter of 3 mm) was thoroughly polished by alumina paste (0.3 μm and 0.05 μm, separately) and sequentially was ultrasonically rinsed in acetone, ethanol and ultrapure water. Then the GCE was dried in N_2 flow. Before immobilizing on bare GCE surface, 8 μL AChE@ZIF-8@Au NPs biocomposites solution was mixed with 4 μL 0.5% CS, and the mixture was mixed thoroughly under shaking for 2 min. Ultimately, the modified electrode (donated as AChE@ZIF-8@Au NPs-CS/GCE) was maintained at 4 °C for drying and further use. For comparison, ZIF-8, ZIF-8@Au NPs, AChE@ZIF-8 were used instead of AChE@ZIF-8@Au NPs to prepare ZIF-8-CS/GCE, ZIF-8@Au NPs-CS/GCE and AChE@ZIF-8-CS/GCE.

2.4. Electrochemical measurements

The electrochemical performance of the fabricated ZIF-8-based electrodes were investigated using electrochemical impedance spectroscopy (EIS) and cyclic voltammetry (CV) techniques. The EIS and CV were monitored in 0.1 M potassium chloride (KCl) solution involving 5 mM $Fe(CN)_6^{3-/4-}$ as a redox detector. Differential pulse voltammetry (DPV) was applied as a tool for the testing of pesticides. The initial DPV signal of the AChE@ZIF-8@Au NPs-CS/GCE to 9 mM ATCh was recorded in PBS (pH 7.0, 0.1 M) solution. Prior to obtaining the inhibited DPV current in a fresh ATCh solution at the same conditions, the AChE electrode was inhibited by a desired concentration of pesticides for 15 min and washed with PBS. The inhibition rate (Inhibit %) could be obtained from formula:

$$Inhibit(\%) = (I_{init} - I_{fin})/I_{init} \times 100\%$$

where I_{init} and I_{fin} represented the peak current before and after inhibition.

3. Results and discussion

3.1. Characterizations of ZIF-8, AChE@ZIF-8 and AChE@ZIF-8@Au NPs

Fig. 1a presented the transmission electron microscope (TEM) morphology of the as-synthesized ZIF-8 crystals, which showed distinct hexagon shape with average size of ~850 nm, and the resulting AChE@ZIF-8 and AChE@ZIF-8@Au biocomposites had the similar morphology to ZIF-8 crystals (Fig. 1b and c). From the XRD patterns in Fig. 2a, we could see that the AChE@ZIF-8 and AChE@ZIF-8@Au biocomposites had the analogous crystal structure with the synthesized ZIF-

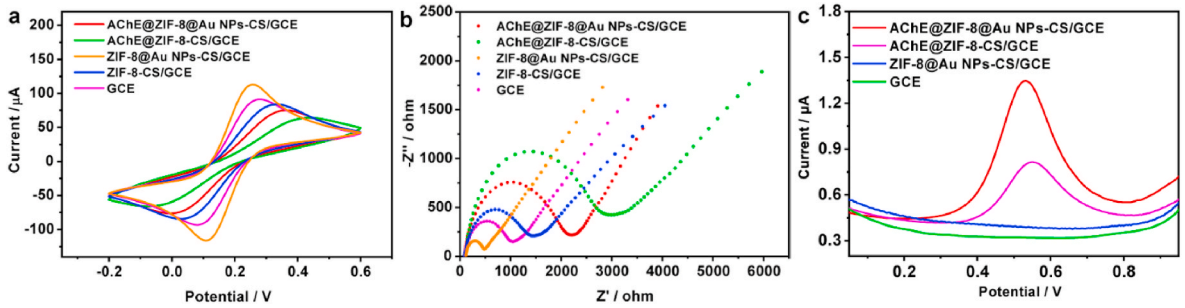

Fig. 3. (a) CV curves, (b) Nyquist plots of bare electrode and modified electrodes in 0.1 M KCl solution with 5 mM $Fe(CN)_6^{3-/4-}$ (Scan rate: 100 mV/s; Frequency range: 0.01 Hz–100 KHz). The semicircle represented the electron-transfer resistance (Ret). (c) DPV responses of different modified electrodes in 0.1 M PBS (pH 7.0) with 9 mM ATCh. (n = 3).

8 and simulated ZIF-8. Moreover, confocal laser scanning microscope (Fig. 1d) was employed for confirming the confinement of FITC-labelled AChE in ZIF-8. Green fluorescence was observed when exciting the FITC-labelled AChE@ZIF-8 biocomposites at 488 nm, and the merged image demonstrated that the AChE was incorporated into ZIF-8 carriers. In addition, to further ascertain that the AChE were biomimetically mineralized within ZIF-8 carriers, fourier transform infrared spectroscopy (FTIR) was performed. As illustrated in Fig. 2b, AChE@ZIF-8 and AChE@ZIF-8@Au NPs showed similar stretches characteristic of the AChE, demonstrating that the AChE were chemically binding within ZIF-8. The porous structures of ZIF-8 and AChE@ZIF-8 were investigated using nitrogen sorption isotherm. The results in Fig. S1 and Table S1 showed that AChE@ZIF-8 possessed lower porosity compared with pure ZIF-8 after the encapsulation of AChE molecules. Additionally, as Fig. 1c displayed, a mass of Au nanoparticles (~4 nm) were uniformly assembled on AChE@ZIF-8, and the lattice fringes of 0.23 nm and 0.20 nm matched with the (111) and (200) planes of Au NPs respectively, demonstrating the successful preparation of AChE@ZIF-8@Au NPs biocomposites. And the existing of gold in biocomposites was also verified by EDS spectrum (Fig. S2). The elemental mapping images in Fig. 1e suggested the evenly distributed of Au NPs on the surface of AChE@ZIF-8.

3.2. Electrochemical behaviors of the modified electrodes

The electrochemical behaviors of different decorated electrodes were investigated by CV and EIS techniques in KCl (0.1 M) and $Fe(CN)_6^{3-/4-}$ (5 mM) mixed solution. As illustrated in Fig. 3a, the bare GCE possessed a typical redox peak. After modifying the bare GCE with ZIF-8, the peak current decreased, which may be caused by the inferior conductivity of ZIF-8. Furthermore, the GCE coated with ZIF-8@Au NPs showed a promoted peak current response and better reversibility compared with ZIF-8-CS/GCE, suggesting that gold nanoparticles can facilitate electron transfer and ameliorate the conductivity of the sensing platform. Whereas, the AChE@ZIF-8@Au NPs or AChE@ZIF-8 biocomposites decorated electrode exhibited the lower peak currents and the worse reversibility than ZIF-8@Au NPs-CS/GCE or ZIF-8-CS/GCE, resulting from the insulating property of enzyme molecule, which also indicated the successful immobilization of AChE on electrode surface. The corresponding EIS curves (Fig. 3b) further revealed the electron-transfer resistance of different electrodes, which agreed well with the CV results.

The electrochemical performance of different modified electrodes towards ATCh was explored using DPV technique. As Fig. 3c displayed, when ATCh was added, no detectable peak current was observed at bare GCE or ZIF-8@Au NPs-CS/GCE, while AChE@ZIF-8@Au NPs-CS/GCE and AChE@ZIF-8-CS/GCE showed obvious current responses, arising from the oxidation of thiocholine (the catalytic product of AChE). Additionally, the AChE@ZIF-8@Au NPs-CS/GCE showed a stronger peak current than AChE@ZIF-8-CS/GCE, possibly caused by the signal amplification effect of Au nanoparticles, because its excellent conductivity facilitated the electron transfer and the inherent catalytic activity promoted the electrocatalytic oxidation of thiocholine [1]. Therefore, the AChE@ZIF-8@Au NPs-CS electrode was used for further investigations.

3.3. Optimization of the measurement conditions

For the sake of achieving better analytical performance of the AChE biosensor, several measurement conditions were optimized. Firstly, the pH value of the PBS buffer was a crucial parameter, which would affect the bioactivity of the enzyme. The relationship between current responses and a series of 0.1 M PBS solutions with pH ranging from 6.0 to 8.5 was investigated. As revealed in Fig. S3a, the maximum peak current appeared at pH 7.0. As a result, we chose pH 7.0 as the best pH value in this work.

The current response of the AChE@ZIF-8@Au NPs-CS/GCE to ATCh was also affected by the amount of Au nanoparticles in the biocomposites. And six different amounts of Au NPs were investigated. Small amounts of Au NPs could not promote the conductivity effectively, while large amounts of Au NPs may aggregate, resulting in blocking the

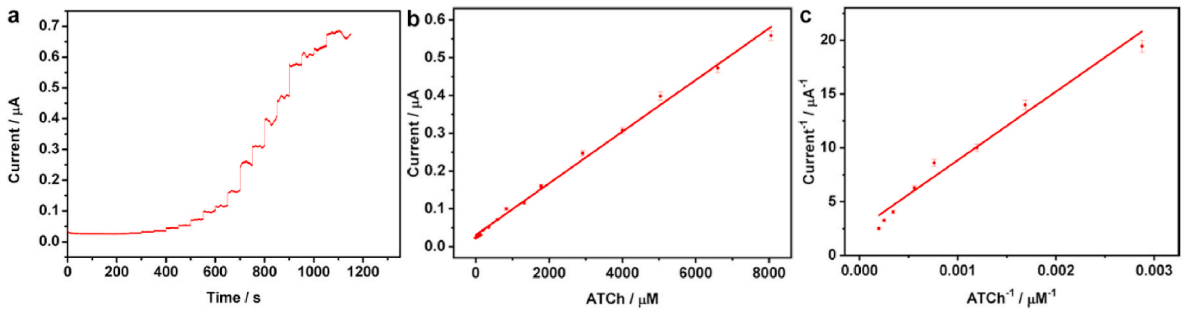

Fig. 4. Amperometric response of AChE-loaded ZIF-8@Au NPs-CS electrode in 0.1 M PBS with the successive injection of ATCh under mild stirring (a); Calibration curve for ATCh determination (b); Lineweaver-Burk plot of 1/current vs. $1/C_{ATCh}$ (c). (n = 3).

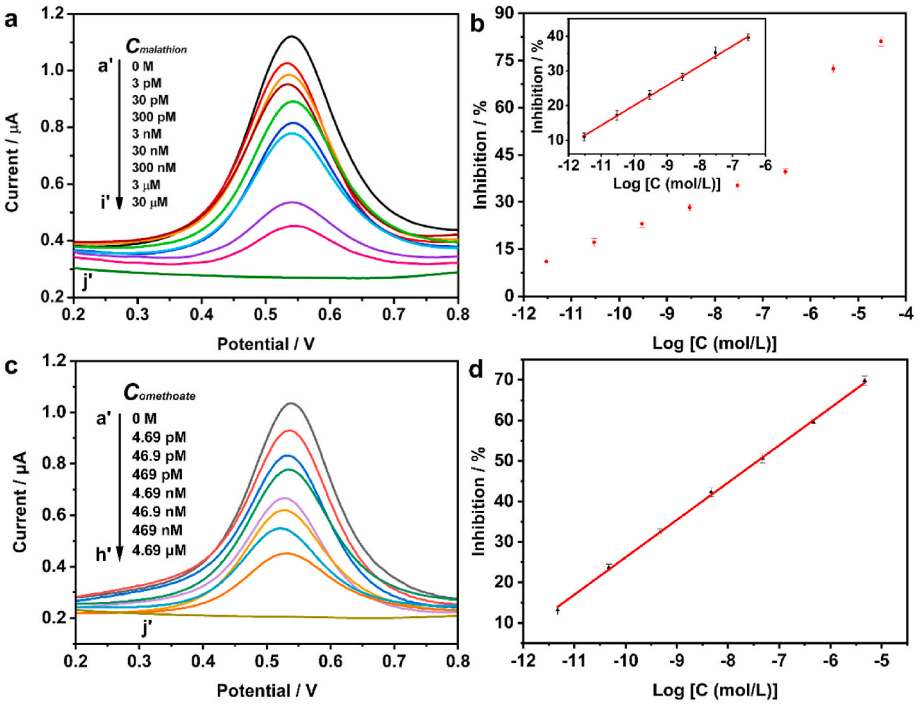

Fig. 5. DPV signals of AChE@ZIF-8@Au NPs-CS/GCE in PBS without ATCh (j') and with ATCh (a'-i') after inhibition with different concentrations of malathion (a) and omethoate (c). Calibration plot for malathion (b) and omethoate (d) detection. (n = 3).

ion channels and reducing the accessibility of ions throughout the electrode surface. As shown in Fig. S4, the optimum amount of Au NPs was obtained as 0.5 mmol.

The volume of the AChE-loaded ZIF-8@Au NPs biocomposites was also studied. As the amount of the biocomposites changing from 2 μL to 15 μL, the current response increased and reached the apex at 8 μL, and then decreased sharply over 8 μL (Fig. S3b). This phenomenon possibly resulted from the excess amount of AChE@ZIF-8 biocomposites, which would hinder the charge transfer. Therefore, 8 μL of the biocomposites was selected as the proper volume in the following experiments.

Furthermore, the incubation time played a crucial role in the performance of AChE biosensor, since the insufficient contact between AChE and pesticides would not thoroughly inhibit the activity of AChE, which led to the inaccuracy in the measurement, whereas a longer incubation time would reduce the effectiveness of real-time monitoring. According to Fig. S3c, the inhibition degree of the pesticides to AChE raised to a plateau as the incubation time exceeded 15 min, resulting from the equilibrium of the binding between the pesticides and the enzyme. Hence, 15 min was utilized as the optimum incubation time.

3.4. Amperometric response towards ATCh

The current-time plot of the AChE@ZIF-8@Au NPs-CS biosensor towards ATCh (Fig. 4) was performed by the continuous injection of ATCh into the 0.1 M PBS buffer system with mild stirring under optimum operation conditions. The current response improved linearly in the ATCh concentration range from 10 μM to 8 mM, together with a linear regression equation of I (μA) = 0.0684 c (mM) + 0.0307 (R = 0.995) (Fig. 4b). When the concentration of ATCh was further raised, a platform appeared, suggesting the Michaelis-Menten process. The Michaelis-Menten constant (K_m), reflecting the enzymatic catalytic activity and affinity [27,28], can be acquired in light of Lineweaver-Burk equation (1) [27,29]. And the K_m value in our study was 2.5 mM, which is lower than 3.1 mM [30].

$$\frac{1}{I_{SS}} = \frac{1}{I_{max}} + \frac{Km}{I_{max}C} \quad (1)$$

3.5. Inhibition effect of malathion

The inhibition effect of pesticides (malathion and omethoate) on enzyme electrodes was investigated by DPV. Fig. 5a and c showed that no current response appeared without ATCh (curve j'), whereas when 9 mM ATCh was added into PBS solution before incubating, an initial peak current was recorded (curve a'). And the current declined gradually after inhibiting the enzyme electrodes by a series of different concentrations of pesticides solution (curves b'-i'), resulted from the reduction of TCh due to the inhibition of AChE activity by pesticides. It can be seen from Fig. 5b and d that the inhibition rate changed linearly with the malathion concentration from 3 pM to 300 nM and the omethoate concentration from 4.69 pM to 4.69 μM and the corresponding linear equations were $Inhibition(\%) = 5.72LogC_{malathion} + 77.16$ ($R^2 = 0.998$) and $Inhibition(\%) = 9.23LogC_{omethoate} + 118.4$ ($R^2 = 0.999$), respectively. And the limit of detection (LOD) were 1.10 pM for malathion and 1.32 pM for omethoate based on S/N = 3. Notably, the obtained LODs far exceed the maximum residue limits (MRLs) for malathion (0.5 mg/kg) and omethoate (0.1 mg/kg) established by European Union, also the LOD values are much lower than the MRLs set by Codex Alimentarius Commission (0.01 mg/kg for malathion and omethoate). Additionally, compared with other reported biosensors [31–39], the AChE@ZIF-8@Au NPs-CS biosensor exhibited comparable linear range and detection limit among the best values (Table S2). This result may be because the porous and biocompatible framework of ZIF-8 could offer an appropriate microenvironment for the encapsulated AChE to maintain its bioactivity [17,18], and the spatial confinement effect provided by ZIF-8 frameworks would probably facilitate enzymatic reactions [13,19]. Moreover, Au nanoparticles with excellent conductivity and intrinsic catalytic activity also contributed to the favorable performance [1].

3.6. Stability

Stability is an important aspect to evaluate the practicability of the biosensor. The amperomeric response of AChE@ZIF-8@Au NPs-CS/GCE

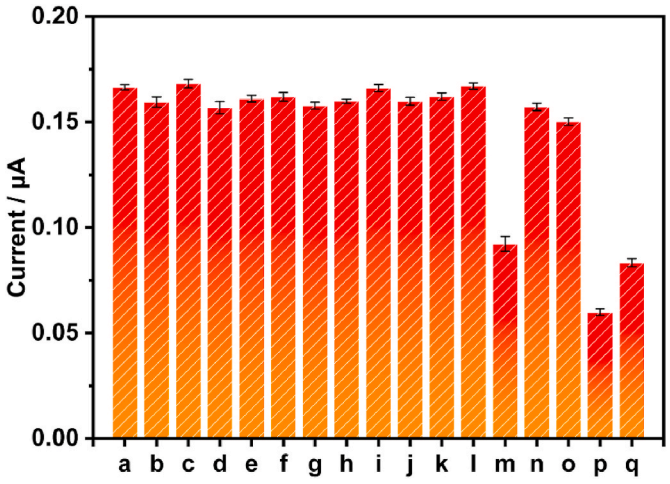

Fig. 6. DPV responses to 3 mM ATCh. (a) Without any interfering species, with 3 mM of different species (b) Mg^{2+}, (c) Co^{2+}, (d) Ni^{2+}, (e) SO_4^{2-}, (f) Cl^-, (g) NO_3^-, (h) urea, (i) citric acid, (j) glucose, (k) *p*-nitroaniline, (l) Pb^{2+}, (m) Cd^{2+}, (n) Zn^{2+}, (o) Cu^{2+}, (p) Cr^{6+} and (q) Hg^{2+}. (n = 3).

to ATCh was measured continuously for 20000s (Fig. S5), and no obvious change of amperomeric response was observed. Additionally, the stability of the fabricated biosensor for different storage periods was researched. And the biosensor displayed negligible change in response current after one-week storage at 4 °C, also it remained 94.65% of its original DPV signal after one month, while some other AChE biosensors suffered a response reduction of 15%–20% after 7-days or one-month storage [10,12,40,41]. The results indicated the satisfactory stability of the proposed biosensor, which should be ascribed to the positive microenvironment created by porous ZIF-8 for AChE through the confinement effect and specific host-guest interactions, which may shelter the AChE molecules from external environments [18,21].

3.7. Precision, anti-interference ability and practical applications

Inter-assay and intra-assay measurements were carried out (see Experimental Details in Supporting Information), and the relative standard deviation (RSD) were 2.39% and 1.56% respectively, implying the acceptable reproducibility and repeatability of the biosensor. Furthermore, in the presence of common interfering compounds (e.g. Mg^{2+}, Co^{2+}, Ni^{2+}, SO_4^{2-}, Cl^-, NO_3^-, urea, glucose, citric acid, *p*-nitroaniline, Pb^{2+}, Zn^{2+} and Cu^{2+}), no significant interferences occurred (Fig. 6). However, Cd^{2+}, Cr^{6+} and Hg^{2+} would severely interfere with the determination. In addition, the practicability of the purposed biosensor was testified using spiked tap water and tomato samples. The recovery for malathion and omethoate detection were calculated to be 100% ± 6% with RSDs <3.9% (Table S3), indicating the good accuracy of the biosensor in real samples analysis.

4. Conclusion

In summary, a stable enzyme immobilization strategy based on AChE@ZIF-8@Au NPs biocomposites was developed for electrochemical determination of pesticides. Due to the advantages of the high porosity of ZIF-8, the excellent conductivity of Au NPs and the confinement of AChE in ZIF-8 framework, satisfying analytical performance (including a wide linear range and a low detection limit), as well as high stability, favorable reproducibility and good recoveries were achieved for malathion determination. Although enhanced stability has been realized by encapsulating the enzymes in MOFs, there are still some limitations. The non-optimized interface between enzymes and MOFs may restrict the catalytic efficiency of enzymes, which could be ameliorated in future by reducing the MOFs framework thickness and modifying the linkers. And the performance of electrochemical biosensors would be further improved via combining with novel advanced nanomaterials since the inferior conductivity of MOFs.

Author contributions

YZ and FG contributed to the conception of the study;
YZ and XL performed the experiment;
YZ and FG performed the data analyses and wrote the manuscript.

Acknowledgements

This work was supported by the National Natural Science Foundation of China (Grant No. 21875205) and the Natural Science Foundation of Hebei Province (Grant No.B2021203016, 206Z4404G).

Appendix A. Supplementary data

Supplementary data to this article can be found online at https://doi.org/10.1016/j.ab.2022.114628.

References

[1] H.F. Cui, T.T. Zhang, Q.Y. Lv, X.J. Song, X.J. Zhai, G.G. Wang, Biosens. Bioelectron. 141 (2019), 111452.
[2] X. Lu, L. Tao, Y.S. Li, H.M. Huang, F.M. Gao, Sensor. Actuator. B Chem. 284 (2019) 103–109.
[3] M.Z.M. Nasir, C.C. Mayorga-Martinez, Z. Sofer, M. Pumera, ACS Nano 11 (2017) 5774–5784.
[4] A. Amine, F. Arduini, D. Moscone, G. Palleschi, Biosens. Bioelectron. 76 (2016) 180–194.
[5] J. Bao, T. Huang, Z. Wang, H. Yang, X. Geng, G. Xu, M. Samalo, M. Sakinati, D. Huo, C. Hou, Sensor. Actuator. B Chem. 279 (2019) 95–101.
[6] X. Lu, L. Tao, D.D. Song, Y. Li, F.M. Gao, Sensor. Actuator. B Chem. 255 (2018) 2575–2581.
[7] L. Ma, L.Y. Zhou, Y. He, L.H. Wang, Z.H. Huang, Y.J. Jiang, J. Gao, Biosens. Bioelectron. 121 (2018) 166–173.
[8] A. Sassolas, L.J. Blum, B.D. Leca-Bouvier, Biotechnol. Adv. 30 (2012) 489–511.
[9] L. Peng, S.Y. Dong, W.B. Wei, X.J. Yuan, T.L. Huang, Biosens. Bioelectron. 92 (2017) 563–569.
[10] D.D. Song, X.Y. Jiang, Y.S. Li, X. Lu, S.R. Luan, Y.Z. Wang, Y. Li, F.M. Gao, J. Hazard Mater. 373 (2019) 367–376.
[11] Y. Wu, L. Jiao, W.Q. Xu, W.L. Gu, C.Z. Zhu, D. Du, Y.H. Lin, Small 15 (2019), 1900632.
[12] G.X. Yu, W.X. Wu, Q. Zhao, X.Y. Wei, Q. Lu, Biosens. Bioelectron. 68 (2015) 288–294.
[13] W.H. Chen, M. Vázquez-González, A. Zoabi, R. Abu-Reziq, I. Willner, Nat. Catal. 1 (2018) 689–695.
[14] X.Z. Lian, Y.P. Chen, T.F. Liu, H.C. Zhou, Chem. Sci. 7 (2016) 6969–6973.
[15] X.Z. Lian, Y. Fang, E. Joseph, Q. Wang, J.L. Li, S.Y. Banerjee, C. Lollar, X. Wang, H. C. Zhou, Chem. Soc. Rev. 46 (2017) 3386–3401.
[16] K. Liang, R. Ricco, C.M. Doherty, M.J. Styles, S. Bell, N. Kirby, S. Mudie, D. Haylock, A.J. Hill, C.J. Doonan, P. Falcaro, Nat. Commun. 6 (2015) 7240.
[17] X.L. Wu, C. Yang, J. Ge, Z. Liu, Nanoscale 7 (2015) 18883–18886.
[18] G. Chen, S.M. Huang, X. Kou, S. Wei, S.Y. Huang, S. Jiang, J. Shen, F. Zhu, G. Ouyang, Angew. Chem. Int. Ed. 58 (2019) 1463–1467.
[19] F.J. Lyu, Y.F. Zhang, R.N. Zare, J. Ge, Z. Liu, Nano Lett. 14 (2014) 5761–5765.
[20] Y.C. Pan, Y.Y. Liu, G.F. Zeng, L. Zhao, Z.P. Lai, Chem. Commun. 47 (2011) 2071–2073.
[21] F.K. Shieh, S.C. Wang, C.I. Yen, C.C. Wu, S. Dutta, L.Y. Chou, J.V. Morabito, P. Hu, M.H. Hsu, K.C.W. Wu, C.K. Tsung, J. Am. Chem. Soc. 137 (2015) 4276–4279.
[22] Z.H. Zhang, H.F. Ji, Y.P. Song, S. Zhang, M.H. Wang, C.C. Jia, J.Y. Tian, L.H. He, X. J. Zhang, C.S. Liu, Biosens. Bioelectron. 94 (2017) 358–364.
[23] Y.J. Du, J. Gao, L.Y. Zhou, L. Ma, Y. He, Z.H. Huang, Y.J. Jiang, Chem. Eng. J. 327 (2017) 1192–1197.
[24] B.K. Ma, L.Z. Cheong, X.C. Weng, C.P. Tan, C. Shen, Electrochim. Acta 283 (2018) 509–516.
[25] X.L. Wu, J. Ge, C. Yang, M. Hou, Z. Liu, Chem. Commun. 51 (2015) 13408–13411.
[26] X.L. Wu, C. Yang, J. Ge, Bioresour. Bioprocess. 4 (2017) 24.
[27] C. Zhai, X. Sun, W.P. Zhao, Z.L. Gong, X.Y. Wang, Biosens. Bioelectron. 42 (2013) 124–130.
[28] H.Y. Zhao, X.P. Ji, B.B. Wang, N. Wang, X.R. Li, R.X. Ni, J.J. Ren, Biosens. Bioelectron. 65 (2015) 23–30.
[29] R.A. Kamin, G.S. Wilson, Anal. Chem. 52 (1980) 1198–1205.
[30] H.F. Cui, W.W. Wu, M.M. Li, X.J. Song, Y.X. Lv, T.T. Zhang, Biosens. Bioelectron. 99 (2018) 223–229.
[31] D. Du, X.X. Ye, J. Cai, J. Liu, A.D. Zhang, Biosens. Bioelectron. 25 (2010) 2503–2508.

[32] L. Ma, Y. He, Y.R. Wang, Y.H. Wang, R.T. Li, Z.H. Huang, Y.J. Jiang, J. Gao, Electrochim. Acta 318 (2019) 525–533.
[33] N.F.M. Rodrigues, S.Y. Neto, R. de C.S. Luz, F.S. Damos, H. Yamanaka, Biosens 8 (2018) 16.
[34] D.D. Song, Y. Li, X. Lu, M.X. Sun, H. Liu, G.M. Yu, F.M. Gao, Anal. Chim. Acta 982 (2017) 168–175.
[35] P. Zhang, T.T. Sun, S.Z. Rong, D.D. Zeng, H.W. Yu, Z. Zhang, D. Chang, H.Z. Pan, Bioelectrochemistry 127 (2019) 163–170.
[36] Z.Z. Zheng, Y.L. Zhou, X.Y. Li, S.Q. Liu, Z.Y. Tang, Biosens. Bioelectron. 26 (2011) 3081–3085.
[37] L. Ma, L.Y. Zhou, Y. He, L.H. Wang, Z.H. Huang, Y.J. Jiang, J. Gao, Electroanalysis 30 (2018) 1801–1810.
[38] Y.S. Zhao, X.L. Li, J.M. Chen, X. Lu, Y.X. Yang, D.D. Song, F.M. Gao, Sensor. Actuator. B. 352 (2022), 131072.
[39] X. Sun, X.Y. Wang, Biosens. Bioelectron. 25 (2010) 2611–2614.
[40] J.W. Ding, H.X. Zhang, F.L. Jia, W. Qin, D. Du, Sensor. Actuator. B Chem. 199 (2014) 284–290.
[41] R.P. Luo, Z.J. Feng, G.N. Shen, Y. Xiu, Y.K. Zhou, X.D. Niu, H.S. Wang, Sens 18 (2018) 4429.